Cancer Genes and Genomics

Molecular Cancer Research

Regulation of Cell Cycle Genes and Induction of Senescence by Overexpression of OTX2 in Medulloblastoma Cell Lines

Jens Bunt, Talitha G. de Haas, Nancy E. Hasselt, Danny A. Zwijnenburg, Jan Koster, Rogier Versteeg, and Marcel Kool

Abstract

The transcription factor orthodenticle homeobox 2 (OTX2) has been implicated in the pathogenesis of medulloblastoma, as it is often highly expressed and sometimes amplified in these tumors. Little is known of the downstream pathways regulated by OTX2. We therefore generated MED8A and DAOY medulloblastoma cell lines with doxycycline-inducible *OTX2* expression. In both cell lines, OTX2 inhibited proliferation and induced a senescence-like phenotype with senescence-associated β-galactosidase activity. Expression profiles of time series after OTX2 induction in MED8A showed early upregulation of cell cycle genes related to the G_2-M phase, such as *AURKA, CDC25C*, and *CCNG2*. Paradoxically, G_1-S phase genes such as *MYC, CDK4, CDK6, CCND1*, and *CCND2* were strongly downregulated, in line with the observed G_1 arrest. ChIP-on-chip analyses of OTX2 binding to promoter regions in MED8A and DAOY showed a strong enrichment for binding to the G_2-M genes, suggesting a direct activation. Their mRNA expression correlated with *OTX2* expression in primary tumors, underscoring the *in vivo* relevance of this regulation. OTX2 induction activated the P53 pathway in MED8A, but not in DAOY, which carries a mutated *P53* gene. In DAOY cells, senescence-associated secretory factors, such as interleukin-6 and insulin-like growth factor binding protein 7, were strongly upregulated after OTX2 induction. We hypothesize that the imbalance in cell cycle stimulation by OTX2 leads to cellular senescence either by activating the P53 pathway or through the induction of secretory factors. Our data indicate that OTX2 directly induces a series of cell cycle genes but requires cooperating genes for an oncogenic acceleration of the cell cycle. *Mol Cancer Res; 8(10); 1344–57. ©2010 AACR.*

Introduction

Medulloblastoma is the most common malignant brain tumor in children and accounts for ~10% of all childhood cancer deaths. Although overall survival rates are improving in recent years, current therapies are still associated with serious long-term side effects, including many cognitive defects. A better understanding of the molecular biology of medulloblastomas is needed to find novel treatment modalities and improve overall survival and quality of life.

One of the genes implicated in medulloblastoma tumorigenesis is orthodenticle homeobox 2 (*OTX2*). SAGE analyses initially identified *OTX2* as highly expressed in medulloblastoma (1). Subsequently, *OTX2* was also found to be strongly amplified in a set of primary tumors and cell lines, suggesting that this gene acts as an oncogene in medulloblastoma (2-4). The *OTX2* gene encodes a member of the bicoid subfamily of homeodomain-containing transcription factors that is essential in brain and sensory organ development (5-7). Mouse models have shown that deletion of both *Otx2* alleles is lethal, whereas decreased levels of Otx2 result in serious malformations of the brain, including cerebellum (5, 8). During cerebellum development, *OTX2* is expressed in proliferating progenitor cells in the external granular cell layer, but expression disappears when these cells migrate to the internal granular cell layer and become fully differentiated (3). No OTX2 was detected in postnatal cerebellum. However, immunohistochemical staining of 152 primary tumors showed OTX2 protein expression in 114 (75%) of all medulloblastomas (3). The OTX2 expression strongly correlated with a classic histology, whereas desmoplastic histology mainly occurred in tumors without OTX2 expression. We recently generated mRNA profiles of 62 medulloblastomas (9). Five molecular subtypes in medulloblastoma were identified with distinct genetic profiles, pathway signatures, and clinicopathologic features. *OTX2* was highly expressed in four subtypes (A, C, D, and E), but is not or only weakly expressed in subtype B. These type B tumors frequently showed desmoplastic histology.

The biological role of OTX2 in these different molecular subtypes of medulloblastoma is still unknown. Silencing *OTX2* expression in medulloblastoma cell lines reduced cell proliferation and tumor formation (4, 10). These data suggest

Authors' Affiliation: Department of Human Genetics, Academic Medical Center, Amsterdam, the Netherlands

Note: Supplementary data for this article are available at Molecular Cancer Research Online (http://mcr.aacrjournals.org/).

Corresponding Author: Marcel Kool, Department of Human Genetics, Academic Medical Center, Meibergdreef 9, P.O. Box 22700, 1100 DE Amsterdam, the Netherlands. Phone: 31-20-566 5170; Fax: 31-20-691-8626. E-mail: m.kool@amc.uva.nl

doi: 10.1158/1541-7786.MCR-09-0546

a crucial role for OTX2 in medulloblastoma, but the transcriptional targets and pathways controlled by OTX2 remain unknown. To investigate OTX2 and downstream pathways, we made use of the MED8A and DAOY medulloblastoma cell lines, which lack endogenous *OTX2* expression. Clones with doxycycline-inducible ectopic *OTX2* expression were generated. *OTX2* overexpression resulted in a reduced cell proliferation and a senescent phenotype. To identify the transcriptional network of OTX2 that may explain the phenotype of OTX2-induced senescence, we performed mRNA profiling of a time series after OTX2 induction in MED8A cells as well as OTX2 chromatin immunoprecipitation followed by promoter array analysis (ChIP-on-chip). Data were validated in DAOY cells with OTX2 induction. Finally, we combined all data with the tumor mRNA profiles to validate the functional OTX2 targets in medulloblastoma tumors.

Materials and Methods

Cell lines, constructs, and transfection procedures

Medulloblastoma cell lines were cultured in DMEM (Richter's modification) (MED8A, UW228-2, D458, D556, and D283) or MEM (DAOY, D425, and D341; Invitrogen), supplemented with 10% fetal bovine serum, 0.1 mmol/L MEM nonessential amino acids, 200 mmol/L glutamine, 100 units/mL penicillin, and 100 μg/mL streptomycin (Invitrogen) at 37°C in a humified atmosphere containing 5% CO_2. To generate OTX2-inducible clones of the MED8A and DAOY cell lines, cells were first transfected with pcDNA6/TR (Invitrogen) expressing the Tet repressor. Lipofectamine 2000 (Invitrogen) was used for all transfections. Transfected cells were cultured in selective medium containing 1 or 4 μg/mL blasticidin (Invitrogen) for DAOY and MED8A, respectively. Surviving clones were tested for high expression of the Tet repressor.

An inducible expression construct of *OTX2* was made by cloning the coding region of *OTX2* (NM_172337) into the pcDNA4/TO/myc-HisA plasmid (Invitrogen). Sequence analysis verified the correct sequence of the construct. This pcDNA4/TO/OTX2 or the pcDNA4/TO/myc-HisA vector was transfected into MED8A and DAOY clones expressing the Tet repressor. Transfected cells were cultured in selective medium with 100 μg/mL zeocin (Invitrogen) to generate stable clones. To induce *OTX2* expression, doxycycline (MP Biochemicals) was added to the cells 24 hours after plating in a final concentration of 100 ng/mL.

Western blotting and antibodies

For preparation of protein extracts, ice-cold buffer containing 10 mmol/L Tris (pH 7.5), 150 mmol/L NaCl, 1% NP40, 1% sodium deoxycholate, 0.1% SDS, complete proteinase inhibitor (Roche Applied Sciences), 0.5 μmol/L NaF, and 0.5 μmol/L Na_3VO_4 was added to the cells. Plates were incubated for 10 minutes on ice. DNA was sheared and lysates were cleared by centrifugation. For cytoplasmic and nuclear fractions, the ProteoExtract Subcellular Proteome Extraction Kit (EMD Chemicals Inc.) was used.

Protein was quantified using the detergent-compatible protein assay (Bio-Rad). SDS-PAGE gels were run with 5 to 30 μg of protein and electroblotted onto an Immobilon-P membrane (Millipore, Billerica). Blocking and incubation were done in 1× TBS with 0.05% Tween 20 and 5% dry milk using standard procedures. OTX2 mouse monoclonal antibody was a gift from Dr. G. Corte (Department of Translational Oncology, National Institute for Cancer Research, Genova, Italy). Other antibodies were commercially obtained: glyceraldehyde-3-phosphate dehydrogenase, phospho-P53, and phospho-extracellular signal–regulated kinase (ERK)-3 (Cell Signaling Technology); histone H3 (Upstate Cell Signaling Solutions); MYC (Roche Applied Sciences); TUBA (Sigma); RB (BD Biosciences); CCND2, CDK4, CDK6, and p-RB (Santa Cruz Biotechnology); CCND1, P16, P21, P27, and P53 (Neomarkers); interleukin-6 (IL-6) and insulin-like growth factor binding protein 7 (IGFBP7; Abcam); and SPRY2 (Abnova). After incubation with a secondary sheep anti-mouse or anti-rabbit horseradish peroxidase–linked antibody (GE Healthcare), proteins were visualized by enhanced chemiluminescence (GE Healthcare).

Growth assay

Uninduced cells and 72-hour induced cells were plated in 96-well microplates. After 4 days, cell viability was measured by adding 25 μL of 3 mg/mL MTT (Sigma) and incubating for 2 to 4 hours at 37°C. Medium was discarded and the remaining precipitate was solubilized by the addition of 50 μL of DMSO. Subsequently, absorbance was measured at 570 and 650 nm (reference) on a Bio-Rad 3550 microplate reader equipped with a spectrophotometer (Bio-Rad). Cell viability was expressed as relative signal compared with uninduced cells, after correction for background absorbance.

Fluorescence-activated cell sorting analysis

For quantification of cell cycle distribution, 100 ng/mL doxycycline was added to cells 24 hours after plating. After 72 hours of induction, cells were trypsinized and washed. Pellet was resuspended in 0.1× PBS containing 7.5 μmol/L propidium iodide and 50 μg/mL RNase A. After a minimal incubation time of 1 hour, cells were analyzed on a BD FACSCanto flow cytometer (BD Bioscience). Obtained data were analyzed using FlowJo 7.2 software (Tree Star, Inc.).

Senescence-associated β-galactosidase staining

To assess senescence-associated β-galactosidase activity, cells were washed with 1× PBS and fixed by incubation in 3% paraformaldehyde. After subsequent washing with 1× PBS, cells were incubated overnight in a 37°C incubator with X-gal staining solution [1 mg/mL X-gal (Invitrogen), 150 mmol/L NaCl, 2 mmol/L $MgCl_2$, 5 mmol/L $K_3Fe(CN)_6$, 5 mmol/L $K_4Fe(CN)_6$ in phosphate buffer (pH 6)]. Pictures were taken using a DMIL microscope with a DC300 camera and IM 500 software (Leica).

RNA extraction and expression profiling

For expression profiling, total RNA was extracted with Trizol reagent (Invitrogen) according to the manufacturer's

instructions. RNA was purified using the RNeasy Mini Kit (Qiagen). RNA quantity and quality were determined by spectrophotometry (Nanodrop) and microfluidics-based electrophoresis (Agilent 2100 Bioanalyzer, Agilent). For Affymetrix microarray analyses, fragmentation of RNA, hybridization to HG U133 Plus 2.0 Array, and scanning were all carried out according to the manufacturer's instructions (Affymetrix, Inc.) at the Microarray Department of the Swammerdam Institute of Life Science of the University of Amsterdam.

Data analyses

All expression data were normalized with the MAS5.0 algorithm of GCOS program (Affymetrix). Target intensity was set to 100 ($\alpha_1 = 0.04$ and $\alpha_2 = 0.06$). Detection *P* values were assigned to each probe set using the MAS5.0 algorithm (trimmed mean 96 = 100). In case of multiple probe sets for one gene, the probe set with the highest expression and correct mapping was used. Publicly available HG U133 Plus 2.0 microarray expression data were obtained from the National Cancer Institute Gene Expression Omnibus database: GSE3526 contains 353 normal tissue samples from the whole body [central nervous system (CNS) and non-CNS; ref. 11]. GSE4290 (12) contains 180 samples derived from normal brain and brain tumor samples (glioblastoma, astrocytoma, and oligodendroglioma). We used only the data for the 153 tumor samples in this series, which were clearly annotated. GSM97826, GSM97836, GSM97858, and GSM97879 were therefore left out. GSE7307 contains expression data for other tumors and normal tissues from different sites. All these data were processed as described above. All analyses were done using the in-house developed software, called R2 (http://r2.amc.nl).[1]

For the MED8A-OTX2 time course, the following criteria applied for genes to be considered significantly regulated. First, the probe set should have minimally 1 present call within the experiment. Second, at least one expression value should exceed an expression value of 50. Finally, compared with $T = 0$, a minimum fold change of 0.5 ^{2}log with $P < 0.00005$ is required. *K*-means clustering was done using the TMEV program (13). Genes were annotated using the Functional Annotation Tool of DAVID (http://niaid.abcc.ncifcrf.gov/; ref. 14). For Gene Ontology enrichment analyses, we used all expressed genes within the experiment as background in these analyses. Enrichment was considered when the enrichment score for levels 4 and 5 in biological processes was higher than 2.5.

To identify genes that correlate with *OTX2* expression *in vivo*, we used the mRNA profiling data of primary tumors (9). Only genes with a minimum of 1 present call were included. Data were extracted using R2 software.[1]

Luciferase assay

To monitor P53 transcriptional activity after OTX2 induction, MED8A-OTX2 and MED8A-control cells were transfected in a 24-well plate with 125 ng of pG13-luc or pM15-luc (kindly provided by Bert Vogelstein, Ludwig Center for Cancer Genetics and Therapeutics, Johns Hopkins Kimmel Cancer Center, Baltimore, MD) using Fugene HD (Roche Applied Sciences; ref. 15). As a normalization control, 20 ng of pGL4.74 (Promega) were included. Luciferase activity was monitored using the dual-luciferase reporter assay kit (Promega) according to the manufacturer's protocol using the Synergy HT Multi-Mode Microplate Reader (BioTek).

P53 mutational analysis

Exons 5 to 8 of *P53* were sequenced using BigDye Terminator v1.1 chemistry (Applied Biosystems; Supplementary Table S7). Sequencing was done on an ABI 3730 capillary sequencer (Applied Biosystems). Electropherograms were analyzed using Codon Code aligner.

ChIP-on-chip analysis

MED8A-OTX2 and DAOY-OTX2 cells incubated for 48 hours with (to induce OTX2) or without doxycycline were cross-linked with 1% formaldehyde for 10 minutes. After washing, cells were incubated for 5 minutes in swelling buffer (5 mmol/L PIPES, 85 mmol/L KCl, 0.5% NP40) and passed through a 23-gauge needle. Isolated nuclei were lysed for 10 minutes in 1 mol/L Tris-HCl/1% SDS/0.5 mol/L EDTA (pH 8) on ice. Lysates were sonicated on ice for 7 × 25 seconds at 30 mA. Three milliliters of sample were diluted 1:10 in 1% Triton X-100/150 mmol/L NaCl/50 mmol/L Tris-HCl/2 mmol/L EDTA and cleared for 30 minutes with 40 μL of protein A-agarose (Roche) and 125 μL of 10 mg/mL haring sperm DNA (Roche). Thirty microliters of OTX2 antibody (Millipore) with 40 μL of beads were added to cleared samples and tumbled overnight in a cold room. The next day, the beads were sequentially washed with 0.1% SDS/1% Triton X-100/150 mmol/L NaCl/20 mmol/L Tris-HCl/2 mmol/L EDTA; with the same solution with 500 mmol/L NaCl; with 1% deoxycholate, 1% NP40/250 mmol/L LiCl/10 mmol/L Tris-HCl/2 mmol/L EDTA; and finally with 10 mmol/L Tris-HCl/10 mmol/L EDTA. DNA was eluted in 500 μL of 100 mmol/L $NaHCO_3$/1% SDS. Twenty microliters of 5 mol/L NaCl were added before de-crosslinking at 65°C for 4 hours. Next, 10 μL of 0.5 mol/L EDTA, 20 μL of 1 mol/L Tris-HCl (pH 6.5), and 2 μL of 10 mg/mL proteinase K (Roche) were added and incubated at 45°C for 1 hour to degrade protein. RNA was degraded by adding 5 μL of 10 mg/mL RNase A (Roche) and incubating for 30 minutes at 37°C. DNA was purified using Qiagen PCR purification kit (Qiagen) and quantified with Quant-IT Picogreen (Invitrogen).

The recovered DNA was amplified for labeling as described previously (16). Labeling of the material, hybridization to the 2.1M Deluxe Promoter Array, scanning of the arrays, and peak calling were performed by Nimblegen, Inc. All peaks as called by the Nimblegen algorithm were assigned to transcriptional start sites (TSS). Peaks were regarded as unique when no peak was detected within a region surrounding a TSS in the control experiment. Raw data were visualized using the R2 program.[1]

[1] J. Koster, personal communication.

Results

OTX2 expression is specific for medulloblastoma

Analysis of mRNA expression data showed that *OTX2* is highly expressed in medulloblastoma, but not in other brain or non-brain tumors or normal tissues (Fig. 1A). Expression profiling of medulloblastoma cell lines showed that five cell lines (D283, D341, D425, D458, and D556) also highly expressed *OTX2*, comparable to the levels observed in tumors (Fig. 1A). Most likely, these cell lines were derived from type E tumors, as they have gain of 17q, expression of *MYC* and retinal genes, and no *CTNNB1* mutations (9, 17). Three cell lines (UW228-2, MED8A, and DAOY) without *OTX2* expression were most likely derived from type B tumors. For instance, they all lack 17q gain, lost 9q (MED8A; ref. 17), were derived from a desmoplastic tumor (DAOY; ref. 18), and all have low *NEUROG1* expression.

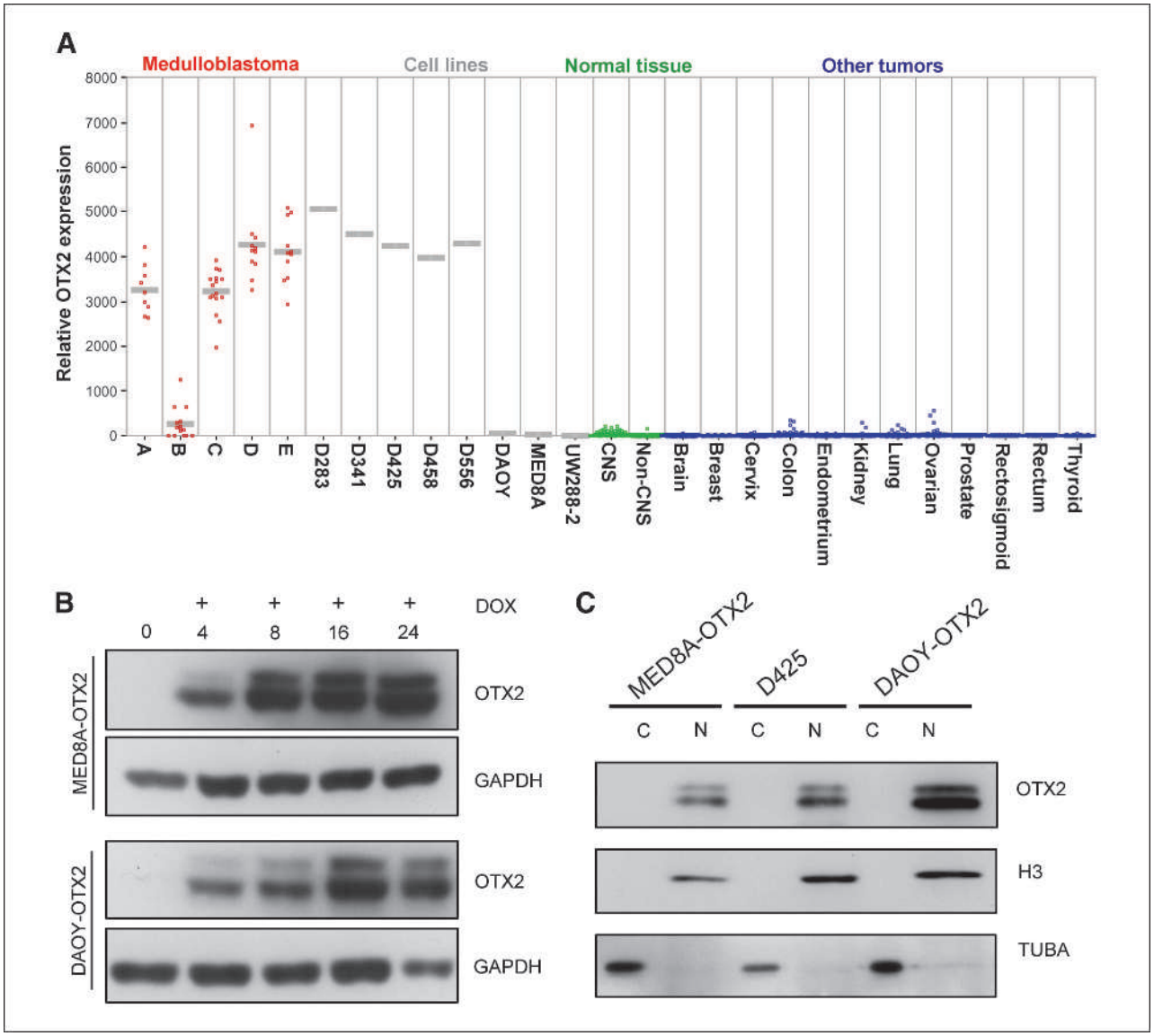

FIGURE 1. *OTX2* expression *in vivo* and *in vitro*. A, *OTX2* mRNA expression in medulloblastoma compared with expression data from 8 medulloblastoma cell lines, 2,207 other tumor samples, and 857 normal tissue samples (see Materials and Methods for references). Similar to tumors, these medulloblastoma cell lines have either very low expression levels (UW228-2, MED8A, and DAOY) or very high expression levels (D458, D425, D556, D341, and D283) of *OTX2*. All expression values represent MAS5.0 normalized data for probe set 242128_at of the Affymetrix HG U133 Plus 2.0 Array. B, OTX2 expression in the nuclei of MED8A-OTX2 and DAOY-OTX2 cells. After addition of 100 ng/mL doxycycline (DOX), OTX2 expression is induced. Within 4 h, in both MED8A-OTX2 and DAOY-OTX2 cells, OTX2 protein can be detected. Within 16 h, OTX2 expression reaches a maximum. Glyceraldehyde-3-phosphate dehydrogenase (GAPDH) was used as a loading control. C, OTX2 expression on Western blot for both cell lines was compared with the endogenous OTX2 protein level of D425 medulloblastoma cell line in the cytoplasm and nucleus. As in the case of D425, OTX2 is only localized in the nucleus of MED8A-OTX2 and DAOY-OTX2 24 h after induction. Also, expression levels are comparable. Histone H3 and TUBA were used as loading controls.

Overexpression of OTX2 in MED8A and DAOY medulloblastoma cell lines

We selected the MED8A and DAOY cell lines (18, 19), which have no endogenous *OTX2* expression, to investigate the effect of OTX2. We generated two clones, MED8A-OTX2 and DAOY-OTX2, which have doxycycline-inducible *OTX2* expression (Fig. 1B). No OTX2 protein expression can be detected in uninduced cells (Fig. 1B) or MED8A and DAOY parental cells (data not shown). OTX2 protein was expressed within 4 hours after addition of doxycycline and reached maximum levels within 24 hours. The induced levels of OTX2 were comparable to the endogenous OTX2 levels in the medulloblastoma cell line D425, which has a strong amplification of the *OTX2* gene (Fig. 1C; refs. 2-4). Moreover, in all three cell lines, OTX2 was detected only in the nuclear fraction (Fig. 1C). The two cell lines with inducible OTX2 therefore represent a good model for the analysis of OTX2 at physiologically relevant levels in medulloblastoma.

OTX2 induces a senescence-like phenotype

OTX2 overexpression reduced the proliferation of MED8A and DAOY cells. After 1 week of OTX2 induction, the number of viable cells was reduced by half in both cell lines compared with uninduced cells (Fig. 2A). However, time course analyses of cell proliferation performed early after OTX2 induction showed that up to 24 hours, cell numbers first slightly increased and, after 48 hours, started to decrease (Supplementary Fig. S1). For MED8A, fluorescence-activated cell sorting analyses revealed that the reduced proliferation was accompanied by a significant increase of cells in G_1-phase, whereas the S and G_2-M fractions decreased (Fig. 2B; Supplementary Fig. S2). In DAOY cells, however, OTX2 induction resulted in a significant increase of cells in G_2-M-phase (Fig. 2B). This difference in cell cycle distribution after OTX2 induction may be related to the difference in P53 status. Sequence analysis showed that MED8A cells are wild-type for P53, but DAOY cells harbor a homozygous P53 mutation (20). We found no indications for increased apoptosis induced by OTX2 because in both cell lines the sub-G_1 fractions did not increase with time, nor did poly(ADP-ribose) polymerase or caspase-3 cleavage (Supplementary Fig. S3). Furthermore, sustained induction of OTX2 in MED8A or DAOY cells resulted in clear morphologic changes. Cells became flattened and showed an increase in the amount of cytoplasm (Fig. 2C). Also, some multinucleated cells were observed. As these features are characteristic of senescent cells, we stained both cell lines for senescence-associated β-galactosidase. β-Galactosidase activity was detected in cells with *OTX2* expression, but not in control cells (Fig. 2D). The presence of this β-galactosidase staining together with the decreased proliferation and change in morphology strongly suggests that OTX2 induces senescence in both medulloblastoma cell lines.

OTX2 induces strong changes in gene expression profile

Because OTX2 is a transcription factor, we were interested in the changes in gene expression after OTX2 induction. A time series analysis of MED8A-OTX2 cells was done using Affymetrix HG U133 Plus 2.0 Arrays. RNA was isolated at 0, 8, 24, and 48 hours after induction of OTX2. Expression of 12,781 genes could be detected in MED8A-OTX2 cells, of which 2,009 were regulated after *OTX2* expression (^{2}log-fold regulation ≥0.5 with $P < 0.00005$; Supplementary Table S1).

OTX2 first stimulates mitotic genes before cells go into senescence

To identify patterns in gene regulation after OTX2 induction, we performed *K*-means clustering on all genes regulated over time. Nine clusters with distinct regulation patterns were identified (Fig. 3). Six clusters (I, III, IV, V, VI, and IX) represent early regulated genes, that is, genes that are up- or down-regulated within 8 hours after OTX2 induction. The genes in the other three clusters are regulated at later time points (II, VII, and VIII). Gene Ontology analysis performed for each gene cluster showed enrichments in specific biological processes for several clusters (Supplementary Table S2; ref. 14). Early induction of specific functional groups was detected in clusters I, IV, and IX. Cluster IX was significantly enriched in genes functioning in mitosis and sister chromosome segregation, such as *AURKA, CDC25C, CCNG2, CENPA*, and *CENPE*. They were rapidly upregulated after OTX2 induction, but their expression decreased again after 24 hours (Fig. 4A). Clusters I and IV, consisting of early regulated genes, were enriched for genes involved in transcription. The late regulated cluster II was significantly enriched for genes involved in ribosome biogenesis and protein translation. Their downregulation may reflect the observed phenotype of reduced proliferation after induction of OTX2. The other five clusters (III, V, VI, VII, and VIII) showed no clear enrichment for biological processes. Similar results were obtained after *K*-means clustering of genes regulated with other cutoff levels (data not shown). These analyses show that although the overexpression of *OTX2* in MED8A cells ultimately leads to growth arrest and senescence, OTX2 may initially stimulate cell cycle progression by inducing G_2-M–related genes. These data are in line with the data for cell proliferation showing that early after OTX2 induction, cell numbers first slightly increased (Supplementary Fig. S1).

OTX2 expression inhibits G_1-S cell cycle progression

Most G_2-M genes that were induced by *OTX2* overexpression in MED8A were highly expressed in all medulloblastomas (Fig. 4A; Supplementary Table S1), suggesting that OTX2 might be responsible for their high expression in tumors. Surprisingly, a group of G_1-S-phase–specific genes, such as *CCND1, CCND2, CDK4, CDK6*, and *MYC*, were all strongly downregulated by OTX2 (Fig. 4B). Nevertheless, these genes are generally highly expressed in medulloblastoma (Fig. 4B; Supplementary Table S1). Strikingly, G_1-S transition inhibitors such as *P15* (*CDKN2B*), *P21* (*CDKN1A*), *P27* (*CDKN1B*), and *P57* (*CDKN1C*) were all upregulated by OTX2 in MED8A (Supplementary Table S1). To validate the

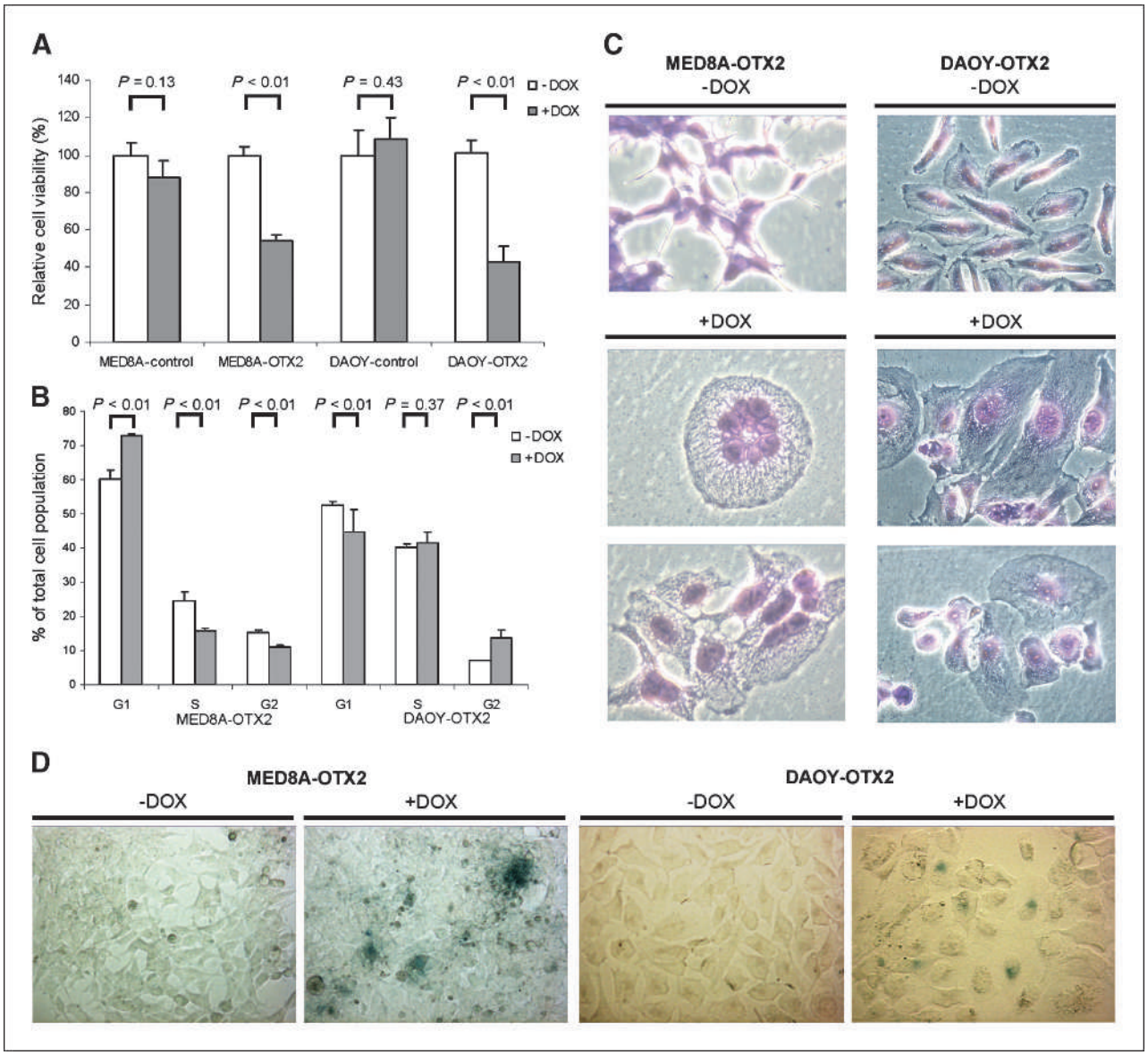

FIGURE 2. Expression of *OTX2* results in reduced cell proliferation, morphologic changes, and senescence-associated β-galactosidase activity. A, *OTX2* expression reduces cell proliferation. MED8A-control, MED8A-OTX2, DAOY-control, and DAOY-OTX2 cells were cultured with or without 100 ng/mL doxycycline. After 3 d, 10,000 (MED8A) or 750 (DAOY) cells were plated in 96-well plates. After 4 d, cell viability was measured by an MTT assay. *OTX2* expressing cells showed a reduced cell proliferation as compared with the controls. B, columns, average cell cycle distribution in MED8A-OTX2 and DAOY-OTX2; bars, SD. After 72 h with or without doxycycline, cells were stained with propidium iodide and analyzed by fluorescence-activated cell sorting. C, cell morphology changes after *OTX2* expression. In both cell lines, cells with *OTX2* expression show enlarged cytoplasm, loss of shape, and multinucleation. Cells were stained with Giemsa after 13 d of culturing with doxycycline. Magnification, ×400 (MED8A-OTX2) or ×200 (DAOY-OTX2). D, senescence-associated β-galactosidase activity was detected in MED8A-OTX2 and DAOY-OTX2 cells 6 d after OTX2 induction, but not in uninduced MED8A or DAOY cells. Magnification, ×200.

paradoxical regulation of G_1-S and G_2-M genes, we analyzed protein lysates from time-series experiments of MED8A-OTX2. The levels of CCND1, CCND2, CDK4, CDK6, and MYC proteins were quickly downregulated after OTX2 induction (Fig. 4C). Despite the differences in cell cycle distribution between MED8A and DAOY cells after OTX2 induction, most of these proteins were also downregulated in DAOY cells (Supplementary Fig. S4). Moreover, protein levels of P21 and P27 were increased in MED8A cells. In DAOY cells, however, which are inhibited in G_2-M, these proteins were not upregulated. Our results show that induction of OTX2 in MED8A cells inhibits the expression of G_1-S-phase genes and, at the same time, stimulates expression of G_2-M genes, suggesting that unbalanced regulation of cell cycle progression might cause oncogenic stress in the cells.

OTX2 expression results in P53 pathway activation in MED8A cells

The P53 pathway is responsive to cell cycle stress and is involved in senescence (21, 22). We therefore asked whether this pathway was activated after OTX2 induction in MED8A cells. Gene Ontology analyses (14) performed for the complete set of regulated genes in the time series identified the P53 pathway as most affected by OTX2, with 23 of its genes being regulated (Supplementary Table S2). Moreover, 32 of 129 direct transcriptional targets of P53 known from literature [as tabulated and reviewed by Riley et al. (23)] were up- or down-regulated in the expected direction when OTX2 was induced (Supplementary Table S1; ref. 23). Examples include *P21, GADD45A*, and *BAX*. Western blot analysis confirmed the increased expression of P21 after OTX2 induction (Fig. 4C). *P53* mRNA levels did not change, but OTX2 induction resulted in increased nuclear levels of P53 protein. Also, a slight increase in P53 phosphorylation was observed, which is known to stabilize the P53 protein (Fig. 5A). To confirm P53 activation after OTX2 induction, we transfected wild-type and mutant reporter constructs for P53 activity into MED8A-OTX2 and MED8A-control cells. The results plotted in Fig. 5B show an up to 4-fold increase in luciferase activity after OTX2 induction in MED8A-OTX2 cells, but not in MED8A-control cells or in MED8A-OTX2 cells transfected with a mutated reporter construct. These data suggest that P53 activity may play a role in the OTX2-induced senescence in MED8A, comparable to the known role of P53 in senescence induced by other oncogenes (21, 22).

OTX2 expression induces senescence-associated secretory factors in DAOY cells

As *P53* and *P16* (*CDKN2A*) are mutated in DAOY cells, the OTX2-induced senescence in these cells must involve other pathways. Senescence-associated secretory factors involved in insulin-like growth factor signaling or inflammation have been shown to play a role in oncogene-induced senescence (24-26). To investigate whether they are involved in the OTX2-induced senescence in DAOY cells, we examined the expression of several candidate secretory factors by Western blot analysis. Indeed, the expression of senescence-associated secretory factors IL-6 (27) and IGFBP7 (28) was strongly increased after OTX2 induction (Fig. 5C). As IL-6 and IGFBP7 signaling have been associated with activated RAS signaling, we also investigated whether RAS signaling was activated after OTX2 induction. Both the levels of phosphorylated ERK and SPRY2, a known target of RAS signaling, were also elevated after OTX2 induction. The levels of phosphorylated RB decreased after OTX2 induction, in line with the observed diminished cell proliferation. These data show that OTX2 induction causes senescence in both medulloblastoma cell lines, but the mechanisms involved are different.

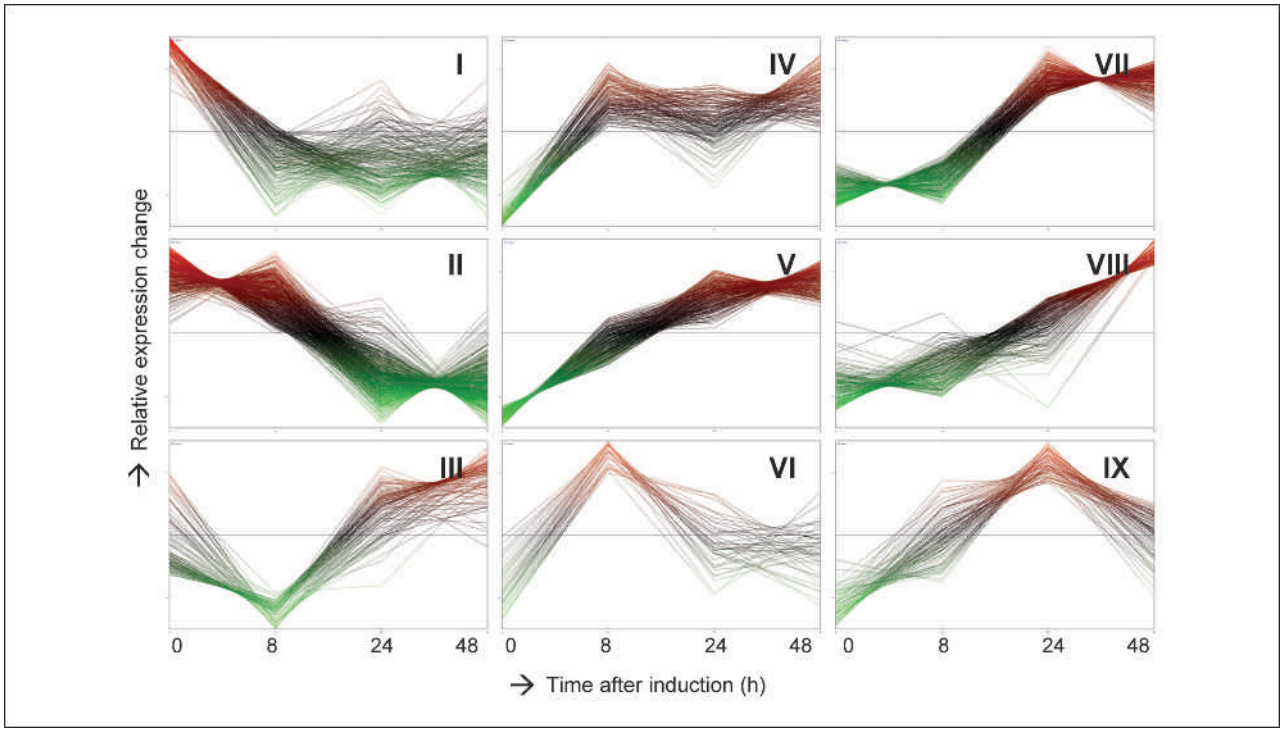

FIGURE 3. Patterns of regulation after *OTX2* expression. *K*-means clustering of the 2,009 genes that were significantly regulated after OTX2 induction in MED8A-OTX2 cell line. The genes were clustered into nine groups using the TMEV software (13). Clusters I, III, IV, V, VI, and IX represent early regulated genes. The other three clusters (II, VII, and VIII) contain genes regulated at later times.

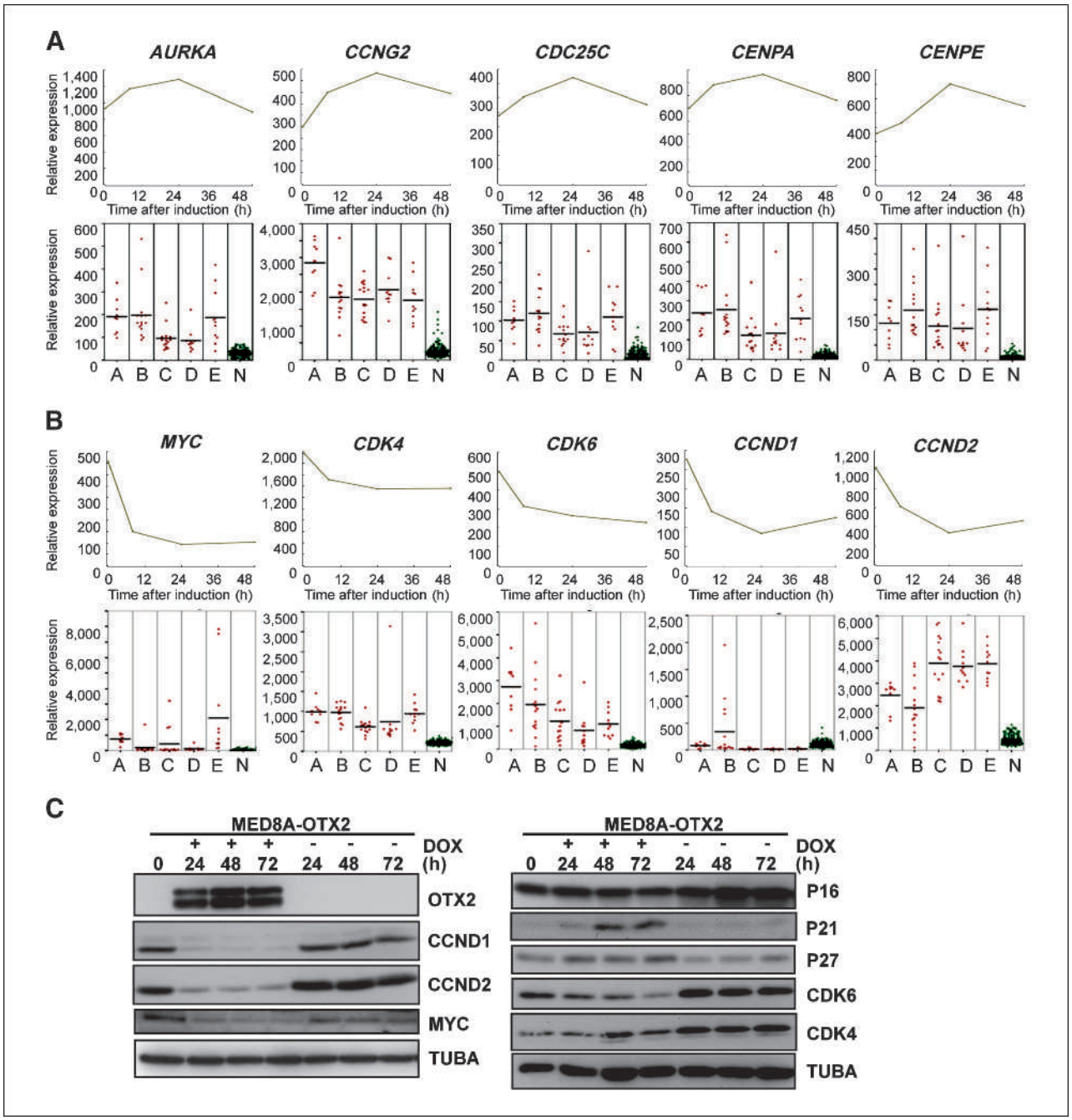

FIGURE 4. *OTX2* overexpression and its effects on cell cycle genes. A, G_2-M–related genes such as *AURKA, CCNG2, CDC25C, CENPA*, and *CENPE* are transiently upregulated after *OTX2* induction. These genes are highly expressed in all tumor subtypes (A-E) compared with 169 normal CNS tissues (N) from GSE3526 (11). B, G_1-S–related genes such as *MYC, CDK4, CDK6, CCND1*, and *CCND2* are downregulated in MED8A-OTX2 cells after *OTX2* induction. These genes are normally highly expressed in medulloblastoma. *MYC* is highly expressed in all tumors of groups A and E and some other cases when compared with normal CNS tissues (N). For *CDK4, CDK6*, and *CCND2*, all tumors show high expression, although expression varies between the subgroups. C, protein levels of cell cycle inhibitors P16, P21, P27, as well as CCND1, CCND2, MYC, CDK4, and CDK6 were determined for MED8A-OTX2 at different time points after induction of OTX2. As expected, by expression profiling, CCND1, CCND2, MYC, CDK4, and CDK6 were found to be downregulated, whereas P21 and P27 levels increased with time. P16 levels did not change. TUBA was used as a loading control.

Mitotic genes are enriched for OTX2 binding

We performed ChIP-on-chip analysis to investigate which genes and processes were likely to be directly regulated by OTX2. Of all expressed genes, 17.6% had one or more significant OTX2 binding peaks in the region around their transcriptional TSSs (250 bp upstream or downstream), but not in the control experiment where OTX2 was not present. A selection of these binding peaks was

validated by quantitative PCR (Supplementary Table S4). Figure 6 shows the OTX2 binding patterns as obtained with the ChIP-on-chip analyses for some representative regulated genes. We analyzed whether the percentage of OTX2 binding was enriched among genes up- or down-regulated after OTX2 induction. OTX2 binding was significantly enriched among regulated genes (20.7%) and even stronger among upregulated genes (22.2%) when compared with nonregulated genes (17.0%; Fig. 7A). Moreover, analysis of the nine clusters of regulated genes identified by *K*-means clustering (Fig. 3) showed a strong enrichment of OTX2 binding (31.8%) for genes in cluster IX, which are associated with mitosis and chromosome segregation. Similar results were obtained when we used larger or smaller regions around the TSSs or different cutoffs for OTX2 binding (data not shown). Our data suggest that OTX2 may function as a transcriptional activator and that genes regulating the mitotic cell cycle are among the direct targets of OTX2.

Gene regulation and OTX2 binding compared with the mRNA data of primary tumors

We analyzed whether genes that correlate in expression with *OTX2* in tumors were enriched for OTX2 binding. We used the mRNA expression profiles of medulloblastoma tumors (9), but excluded the profiles of type A and type B tumors. Type B tumors, characterized by activated SHH signaling, have no or very low *OTX2* expression. Including these tumors would result in many genes that correlate with *OTX2* expression but, in fact, represent subtype-specific differences not related to OTX2. Type A tumors, characterized by activated WNT signaling, were excluded because of the very different genetic background compared with other subtypes.

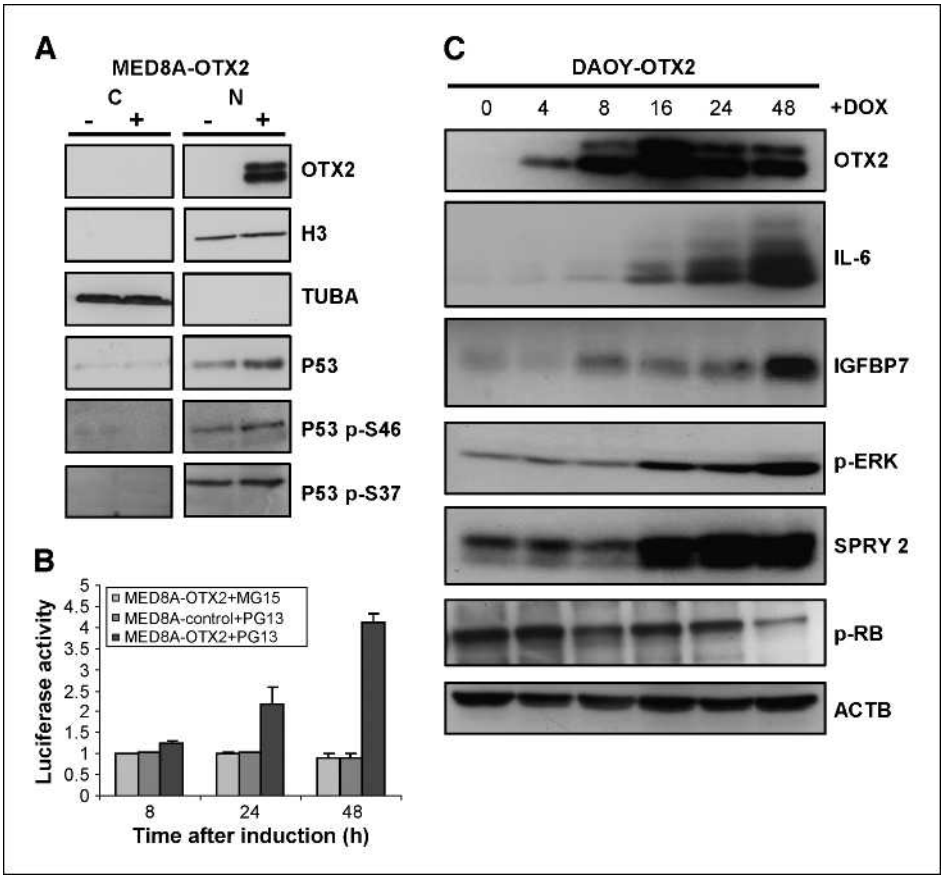

FIGURE 5. Different senescence-associated pathways activated after OTX2 induction. A, cytoplasmic and nuclear fractions were isolated in MED8A-OTX2 24 h after induction. Total nuclear as well as phospho-serine 37 (p-S37) and phospho-serine 46 (p-S46) levels of P53 increased after induction of OTX2. Histone H3 and TUBA were used as loading controls. B, firefly luciferase reporters containing multiple copies of consensus (PG13-Luc) or mutant P53-binding sites (MG15-luc) along with internal control Renilla luciferase reporter were transfected into MED8A-OTX2 or MED8A-control cells. Dual luciferase assays were carried out at different time points. Firefly luciferase activity was normalized against Renilla luciferase activity. The relative luciferase activity of induced cells over uninduced cells was plotted with the basal activity at 0 h set as 1. Only the luciferase activity of PG13-Luc in MED8A-OTX2 cells increased. C, Western blot analyses of senescence-associated secretory factors in DAOY-OTX2 cells after OTX2 induction. Protein levels of IL-6 and IGFBP7 were determined for DAOY-OTX2 at different time points after induction of OTX2. Also, the RAS-ERK pathway was activated after OTX2 induction, as shown by elevated levels of p-ERK and SPRY2. Furthermore, p-RB levels decreased, indicating an impaired G_1-S transition. ACTB was used as a loading control.

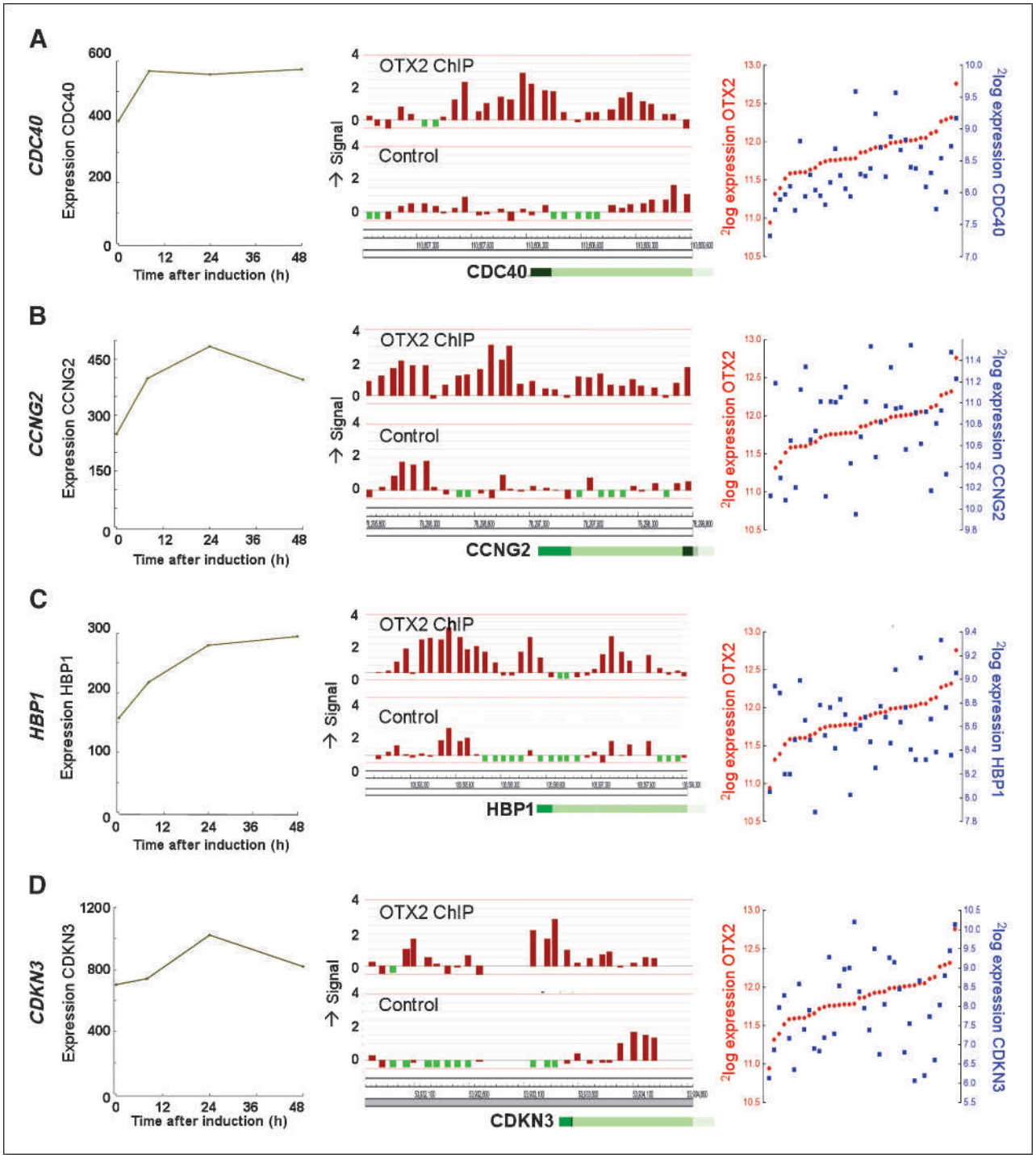

FIGURE 6. Examples of regulated genes with OTX2 binding and their correlation with *OTX2* expression in tumors. *CDC40* (A), *CCNG2* (B), *HBP1* (C), and *CDKN3* (D) represent genes upregulated by OTX2 in MED8A-OTX2 (first panel), with direct OTX2 binding near the TSS (second panel), and a corresponding positive correlation with *OTX2* in primary medulloblastoma (third panel). All these genes are involved in cell cycle regulation.

Of all genes expressed in C, D, and E (CDE) tumors, 17.1% showed binding of OTX2 in MED8A cells (Fig. 7B). Genes that positively correlate with *OTX2* expression in CDE tumors were enriched for *OTX2* binding, and this enrichment increased to >25% when we used more stringent cutoffs for correlation with *OTX2* expression (Fig. 7B). In contrast, genes that negatively correlate with *OTX2* expression were not enriched for OTX2 binding

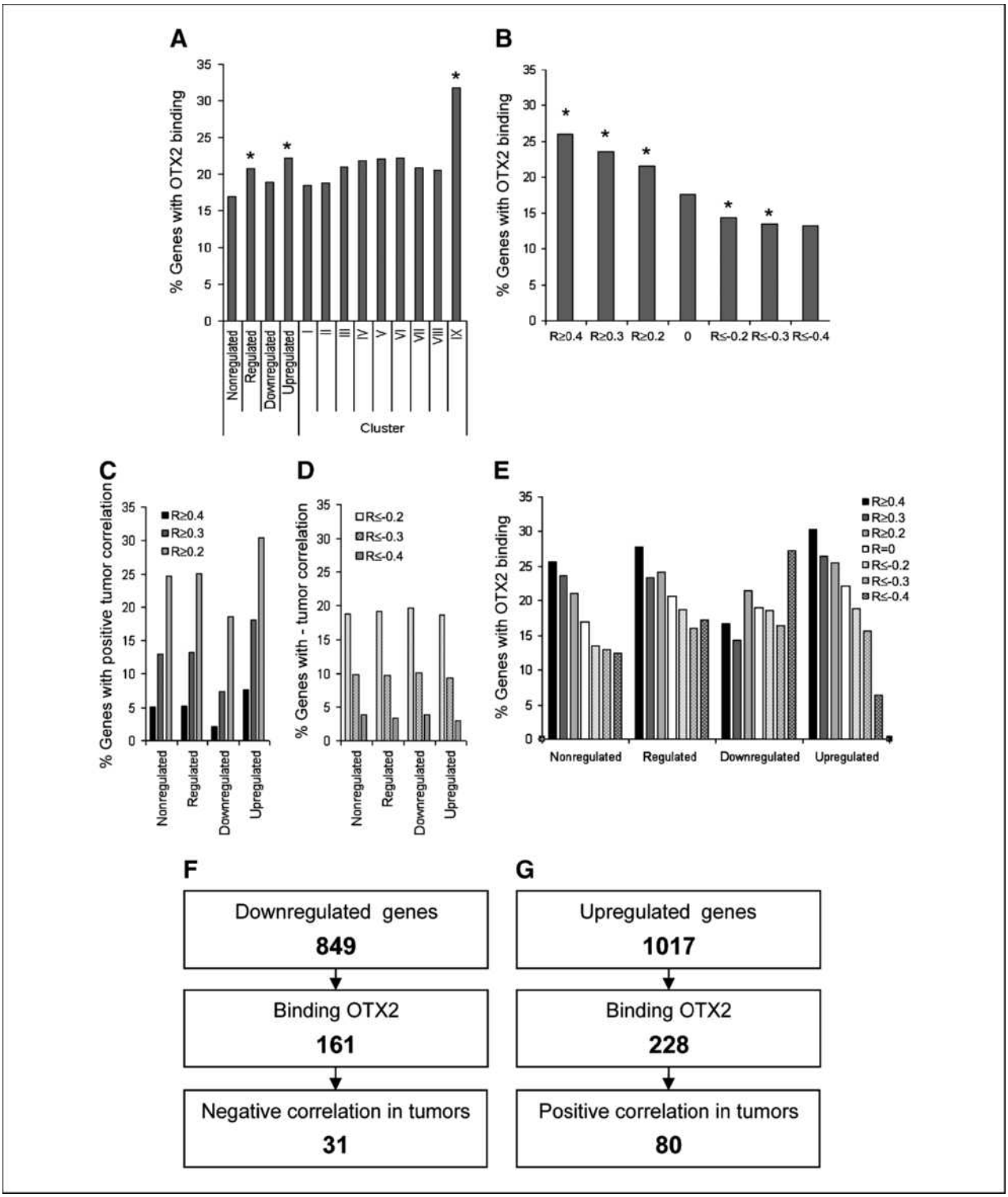

FIGURE 7. Relationship between genes regulated by OTX2, OTX2-bound genes, and genes that correlate with *OTX2* expression in tumors. A, OTX2-regulated genes in MED8A are enriched for OTX2 binding near TSS. This enrichment is most clear among upregulated genes, especially for genes in cluster IX. B, similarly, genes with increasing positive correlation with *OTX2* in primary tumors also show more OTX2 binding in the MED8A-OTX2 ChIP-on-chip experiment. C, upregulated genes in MED8A-OTX2 cells strongly overlap with genes that positively correlate with *OTX2* expression in primary tumors. D, the overlap between downregulated genes and genes that negatively correlate with *OTX2* expression is much smaller. E, all data sets combined. OTX2 binding near TSS is most prominent in genes upregulated in MED8A-OTX2 and with a positive correlation in primary tumors. F and G, identification of regulated genes that bind OTX2 and correlate with *OTX2* expression in tumors ($R \geq 0.2$). *, $P < 0.0001$, χ^2 test with Yates correction.

and even showed lower percentages of OTX2 binding. We also analyzed the overlap between genes that are regulated by OTX2 in MED8A cells and genes that correlate with *OTX2* expression in tumors. The strongest overlap was found for genes that are upregulated by OTX2 in MED8A cells and that positively correlate in tumors (Figs. 6 and 7C and D; Supplementary Table S5). Finally, we combined all parameters (regulation in MED8A, binding by OTX2, and correlation in tumors; Fig. 7E). Genes upregulated in MED8A cells and with a positive correlation with *OTX2* in tumors were clearly enriched for OTX2 binding (30.4%). This was not the case for downregulated genes. These data support our previous analyses of gene regulation by OTX2 in MED8A cells, suggesting that, *in vivo*, OTX2 also mainly functions as a transcriptional activator.

Mitotic genes are among the most promising direct targets of OTX2

To identify which of the regulated genes in MED8A are most likely direct targets of OTX2 in medulloblastoma, we combined all data (Supplementary Table S6). Thirty-one genes were downregulated and bound by OTX2 and had a negative correlation with *OTX2* expression in tumors (Fig. 7F). Eighty genes were upregulated and bound by OTX2 and had a positive correlation in tumors (Fig. 7G). As expected, the upregulated genes include several G_2-M–associated genes, such as *CDC25C, CCNG2, RCBTB1, DSN1, NDE1, SGOL2, CDC40, CEP57*, and *CEP70* (Fig. 6). Strikingly, this list also includes genes that negatively regulate the G_1-S transition, such as *HBP1, E2F8*, and *CDKN3* (Fig. 6). Moreover, *GSPT1*, which is necessary for G_1-S transition, is one of the downregulated genes. Overall, these candidate OTX2 targets seem to promote G_2-M while inhibiting G_1-S transition.

To evaluate whether these stringently selected genes were also regulated by OTX2 in DAOY cells, we selected nine genes, upregulated after OTX2 induction in MED8A cells, and analyzed their expression by quantitative PCR in DAOY cells after OTX2 induction. This analysis showed that OTX2 also induced their expression in DAOY cells (Supplementary Figs. S5 and S6). Furthermore, we performed an OTX2 ChIP-on-chip experiment on OTX2-induced DAOY cells. OTX2 binding was detected for 20% of all genes, but this percentage increased to 61% for genes that were regulated and bound by OTX2 in the MED8A cells. This percentage of OTX2 binding even further increased to 68% for genes that also correlated in expression with *OTX2* in primary tumors (Supplementary Table S6). These data strongly suggest that many of the genes regulated in MED8A after OTX2 induction are also directly regulated by OTX2 in DAOY.

Discussion

Ectopic expression of *OTX2* at physiologic levels in MED8A and DAOY medulloblastoma cell lines resulted in reduced cell proliferation. Both cell lines displayed an oncogene-induced senescence-like phenotype characterized by increased cytoplasm, loss of shape, and senescence-associated β-galactosidase activity. The OTX2-induced senescence explains why, in the past, we failed to generate constitutively *OTX2*-expressing cell lines of both MED8A and DAOY cells. OTX2-induced senescence was not anticipated, as both cell lines that have no endogenous *OTX2* express low levels of *OTX1*, which encodes a functional homologue of OTX2 (29). Medulloblastoma tumors without *OTX2* expression also have *OTX1* expression, although in most cases at low levels (3). However, the proliferation of MED8A and DAOY cells was apparently not compatible with high OTX2 levels. Nevertheless, we identified genes regulated and bound by OTX2 in MED8A-OTX2 cells that show a clear correlation with *OTX2* expression in tumors (Fig. 7F and G; Supplementary Tables S1 and S6). Many of these genes were also regulated and bound by OTX2 in DAOY cells.

Oncogene-induced senescence was first described in cells with overexpression of constitutively activated *RAS* genes (30). These oncogenes are able to transform cells, but only in collaboration with other oncogenes such as *MYC* (31, 32). Similar results have been described for ectopic expression of other components of the RAS pathway, such as *RAC1* and *RAF* (33, 34), as well as other oncogenes, including *E2F* and *STAT5A* (35, 36). Although, in most studies, these experiments were conducted in primary fibroblasts or other primary cell lines, oncogene-induced senescence has also been described in tumor cell lines (37, 38). The molecular mechanisms underlying oncogene-induced senescence are complex, but most signals seem to converge on the RB and P53 pathways (22), as observed in MED8A cells. Accordingly, virtually all human cancers lack functional RB and P53 pathways and thereby escape from senescence (39). Alternative mechanisms of oncogene-induced senescence involve the activation of senescence-associated secretory factors (24-26), as observed in DAOY cells after OTX2 induction for IL-6 (27) and IGFBP7 (28). Interestingly, these secretory factors were not activated in MED8A cells after OTX2 induction (Supplementary Table S1), most likely because they were suppressed by P53 (40).

Expression profiling of MED8A cells showed that, among many others, mitosis-related genes were initially upregulated, followed by a decrease at later time points (cluster IX of Figs. 3 and 4A). Furthermore, these genes were enriched for OTX2 binding to the TSS region and for positive correlation with *OTX2* expression in tumors (Fig. 7A and C), suggesting that they represent direct targets of OTX2. These data further hint at an initial stimulation of cell proliferation. Such an effect has been described for other oncogenes that induce senescence (35, 41, 42). We also observed a slight increase in cell proliferation shortly after OTX2 induction in MED8A and DAOY cells before the onset of senescence and reduced cell proliferation (Supplementary Fig. S1). This initial increase in proliferation in our model is modest,

which might be due to the higher basal proliferation rates of cancer cells relative to the fibroblast cells used in other studies. In addition, already early after OTX2 induction, G_1-S cell cycle genes were downregulated (Fig. 4B and C). This imbalance in cell cycle regulation by OTX2 probably creates stress that leads to P53 pathway activation, such as in MED8A cells, or, when P53 is mutated, to activation of senescence-associated secretory factors, such as in DAOY cells. Expression profiling and reporter assays of MED8A cells showed activation of P53 and its downstream target genes after induction of OTX2.

Most medulloblastomas express high *OTX2* levels (9). We hypothesize that inactivation of the P53 pathway is one of the potential mechanisms in medulloblastoma to prevent OTX2-induced senescence. However, *P53* mutation or amplification of *MDM2*, which inhibits P53, has been infrequently reported for medulloblastoma (20, 43-46). However, *PPM1D*, shown to inhibit P53 in medulloblastoma, is highly overexpressed in most medulloblastoma and even amplified in some (9, 47-49).

Furthermore, to prevent an imbalance in cell cycle regulation induced by OTX2, medulloblastomas must have found ways to drive G_1-S transition. *CCND1, CCND2, CDK4, CDK6*, and *MYC* are all highly expressed in medulloblastoma (Fig. 4B; Supplementary Table S1). In some tumors, this is caused by gene amplifications (9, 49, 50). Especially *MYC*, but also its family members *MYCN* and *MYCL*, are frequently amplified in medulloblastomas (9, 51). If not amplified, these genes are transcriptionally upregulated as direct targets of the WNT or SHH signaling pathway, which are constitutively activated in ~40% of medulloblastomas (9, 52).

The potential role of OTX2 as a positive regulator of cell cycle progression, as suggested by the regulation of mitosis genes, fits with our observation that, in normal cerebellum, OTX2 is mainly expressed in proliferating progenitor cells, but not in differentiated neurons (3). It is also in line with the results reported by Yan and colleagues that silencing of *OTX2* in D425 cells inhibited proliferation and induced differentiation (4, 10). However, ectopic expression of *OTX2* alone is apparently not sufficient to drive proliferation and instead results in senescence in both MED8A and DAOY cells. Here, we present the first data about the genes and pathways regulated by OTX2. OTX2 directly and indirectly upregulates genes associated with the G_2-M phase of the cell cycle. These data are confirmed in D425 cells in which we silenced *OTX2* expression using inducible shRNA. Microarray and OTX2 ChIP-on-chip analyses performed for these cells also identified the mitotic cell cycle genes as one of the major categories of direct targets of OTX2. The full description of these data will be published elsewhere.[2] Our results emphasize the role of *OTX2* as an oncogene. In addition, our data obtained with MED8A and DAOY cells also suggest that cooperating genes are required for a balanced acceleration of the cell cycle by OTX2 in medulloblastoma.

Disclosure of Potential Conflicts of Interest

No potential conflicts of interest were disclosed.

Acknowledgments

We thank Sonia Tosheva, R. Volckmann, and P. van der Sluis for their technical support; T. van der Hoeven and J. Verkooijen for the microarray hybridizations; and M. Hamdi for scientific advice.

Grant Support

Stichting Kindergeneeskundig Kankeronderzoek.

The costs of publication of this article were defrayed in part by the payment of page charges. This article must therefore be hereby marked *advertisement* in accordance with 18 U.S.C. Section 1734 solely to indicate this fact.

Received 12/23/2009; revised 08/17/2010; accepted 09/03/2010; published OnlineFirst 09/13/2010.

[2] Bunt J, Hasselt NE, Zwijnenburg DA, Hamdi M, Koster J, Versteeg R, Kool M. OTX2 drives medulloblastoma proliferation via direct regulation of cell cycle genes and inhibits differentiation. Submitted for publication.

References

1. Michiels EM, Oussoren E, Van Groenigen M, et al. Genes differentially expressed in medulloblastoma and fetal brain. Physiol Genomics 1999;1:83–91.
2. Boon K, Eberhart CG, Riggins GJ. Genomic amplification of orthodenticle homologue 2 in medulloblastomas. Cancer Res 2005;65:703–7.
3. de Haas T, Oussoren E, Grajkowska W, et al. OTX1 and OTX2 expression correlates with the clinicopathologic classification of medulloblastomas. J Neuropathol Exp Neurol 2006;65:176–86.
4. Di C, Liao S, Adamson DC, et al. Identification of OTX2 as a medulloblastoma oncogene whose product can be targeted by all-*trans* retinoic acid. Cancer Res 2005;65:919–24.
5. Acampora D, Mazan S, Lallemand Y, et al. Forebrain and midbrain regions are deleted in Otx2$^{-/-}$ mutants due to a defective anterior neuroectoderm specification during gastrulation. Development 1995;121:3279–90.
6. Martinez S. The isthmic organizer and brain regionalization. Int J Dev Biol 2001;45:367–71.
7. Morsli H, Tuorto F, Choo D, Postiglione MP, Simeone A, Wu DK. Otx1 and Otx2 activities are required for the normal development of the mouse inner ear. Development 1999;126:2335–43.
8. Fossat N, Chatelain G, Brun G, Lamonerie T. Temporal and spatial delineation of mouse Otx2 functions by conditional self-knockout. EMBO Rep 2006;7:824–30.
9. Kool M, Koster J, Bunt J, et al. Integrated genomics identifies five medulloblastoma subtypes with distinct genetic profiles, pathway signatures and clinicopathological features. PLoS ONE 2008;3:e3088.
10. Adamson DC, Shi Q, Wortham M, et al. OTX2 is critical for the maintenance and progression of Shh-independent medulloblastomas. Cancer Res 2010;70:181–91.
11. Roth RB, Hevezi P, Lee J, et al. Gene expression analyses reveal molecular relationships among 20 regions of the human CNS. Neurogenetics 2006;7:67–80.
12. Sun L, Hui AM, Su Q, et al. Neuronal and glioma-derived stem cell factor induces angiogenesis within the brain. Cancer Cell 2006;9:287–300.

13. Saeed AI, Sharov V, White J, et al. TM4: a free, open-source system for microarray data management and analysis. Biotechniques 2003; 34:374–8.
14. Dennis G, Jr., Sherman BT, Hosack DA, et al. DAVID: Database for Annotation, Visualization, and Integrated Discovery. Genome Biol 2003;4:3.
15. El Deiry WS, Kern SE, Pietenpol JA, Kinzler KW, Vogelstein B. Definition of a consensus binding site for p53. Nat Genet 1992;1:45–9.
16. Ren B, Robert F, Wyrick JJ, et al. Genome-wide location and function of DNA binding proteins. Science 2000;290:2306–9.
17. Langdon JA, Lamont JM, Scott DK, et al. Combined genome-wide allelotyping and copy number analysis identify frequent genetic losses without copy number reduction in medulloblastoma. Genes Chromosomes Cancer 2006;45:47–60.
18. Jacobsen PF, Jenkyn DJ, Papadimitriou JM. Establishment of a human medulloblastoma cell line and its heterotransplantation into nude mice. J Neuropathol Exp Neurol 1985;44:472–85.
19. Waha A, Waha A, Koch A, et al. Epigenetic silencing of the HIC-1 gene in human medulloblastomas. J Neuropathol Exp Neurol 2003; 62:1192–201.
20. Raffel C, Thomas GA, Tishler DM, Lassoff S, Allen JC. Absence of p53 mutations in childhood central nervous system primitive neuroectodermal tumors. Neurosurgery 1993;33:301–5.
21. Collado M, Serrano M. The power and the promise of oncogene-induced senescence markers. Nat Rev Cancer 2006;6:472–6.
22. Courtois-Cox S, Jones SL, Cichowski K. Many roads lead to oncogene-induced senescence. Oncogene 2008;27:2801–9.
23. Riley T, Sontag E, Chen P, Levine A. Transcriptional control of human p53-regulated genes. Nat Rev Mol Cell Biol 2008;9:402–12.
24. Cichowski K, Hahn WC. Unexpected pieces to the senescence puzzle. Cell 2008;133:958–61.
25. Chandeck C, Mooi WJ. Oncogene-induced cellular senescence. Adv Anat Pathol 2010;17:42–8.
26. Kuilman T, Peeper DS. Senescence-messaging secretome: SMS-ing cellular stress. Nat Rev Cancer 2009;9:81–94.
27. Kuilman T, Michaloglou C, Vredeveld LC, et al. Oncogene-induced senescence relayed by an interleukin-dependent inflammatory network. Cell 2008;133:1019–31.
28. Wajapeyee N, Serra RW, Zhu X, Mahalingam M, Green MR. Oncogenic BRAF induces senescence and apoptosis through pathways mediated by the secreted protein IGFBP7. Cell 2008; 132:363–74.
29. Acampora D, Annino A, Puelles E, Alfano I, Tuorto F, Simeone A. OTX1 compensates for OTX2 requirement in regionalisation of anterior neuroectoderm. Gene Expr Patterns 2003;3:497–501.
30. Serrano M, Lin AW, McCurrach ME, Beach D, Lowe SW. Oncogenic ras provokes premature cell senescence associated with accumulation of p53 and p16(INK4a). Cell 1997;88:593–602.
31. Malumbres M, Barbacid M. RAS oncogenes: the first 30 years (vol 3, pg 459, 2003). Nat Rev Cancer 2003;3:708.
32. Zhuang D, Mannava S, Grachtchouk V, et al. C-MYC overexpression is required for continuous suppression of oncogene-induced senescence in melanoma cells. Oncogene 2008;27:6623–34.
33. Debidda M, Williams DA, Zheng Y. Rac1 GTPase regulates cell genomic stability and senescence. J Biol Chem 2006;281:38519–28.
34. Zhu JY, Woods D, McMahon M, Bishop JM. Senescence of human fibroblasts induced by oncogenic Raf. Genes Dev 1998;12: 2997–3007.
35. Lazzerini DE, Attwooll C, Pasini D, Helin K. Deregulated E2F activity induces hyperplasia and senescence-like features in the mouse pituitary gland. Mol Cell Biol 2005;25:2660–72.
36. Mallette FA, Gaumont-Leclerc MF, Huot G, Ferbeyre G. Myc down-regulation as a mechanism to activate the Rb pathway in STAT5A-induced senescence. J Biol Chem 2007;282:34938–44.
37. Ravi RK, McMahon M, Yangang Z, et al. Raf-1-induced cell cycle arrest in LNCaP human prostate cancer cells. J Cell Biochem 1999;72:458–69.
38. Bihani T, Mason DX, Jackson TJ, Chen SC, Boettner B, Lin AW. Differential oncogenic Ras signaling and senescence in tumor cells. Cell Cycle 2004;3:1201–7.
39. Sherr CJ, McCormick F. The RB and p53 pathways in cancer. Cancer Cell 2002;2:103–12.
40. Coppe JP, Desprez PY, Krtolica A, Campisi J. The senescence-associated secretory phenotype: the dark side of tumor suppression. Annu Rev Pathol 2010;5:99–118.
41. Di Micco R, Fumagalli M. Breaking news: high-speed race ends in arrest-how oncogenes induce senescence. Trends Cell Biol 2007; 17:529–36.
42. Grandori C, Wu KJ, Fernandez P, et al. Werner syndrome protein limits MYC-induced cellular senescence. Genes Dev 2003;17: 1569–74.
43. Adesina AM, Nalbantoglu J, Cavenee WK. p53 gene mutation and mdm2 gene amplification are uncommon in medulloblastoma. Cancer Res 1994;54:5649–51.
44. Badiali M, Iolascon A, Loda M, et al. p53 gene mutations in medulloblastoma. Immunohistochemistry, gel shift analysis, and sequencing. Diagn Mol Pathol 1993;2:23–8.
45. Cogen PH, Daneshvar L, Metzger AK, Duyk G, Edwards MS, Sheffield VC. Involvement of multiple chromosome 17p loci in medulloblastoma tumorigenesis. Am J Hum Genet 1992;50:584–9.
46. Tong CY, Hui AB, Yin XL, et al. Detection of oncogene amplifications in medulloblastomas by comparative genomic hybridization and array-based comparative genomic hybridization. J Neurosurg 2004; 100:187–93.
47. Castellino RC, De Bortoli M, Lu X, et al. Medulloblastomas overexpress the p53-inactivating oncogene WIP1/PPM1D. J Neurooncol 2008;86:245–56.
48. Ehrbrecht A, Muller U, Wolter M, et al. Comprehensive genomic analysis of desmoplastic medulloblastomas: identification of novel amplified genes and separate evaluation of the different histological components. J Pathol 2006;208:554–63.
49. Mendrzyk F, Radlwimmer B, Joos S, et al. Genomic and protein expression profiling identifies CDK6 as novel independent prognostic marker in medulloblastoma. J Clin Oncol 2005;23:8853–62.
50. Rollbrocker B, Waha A, Louis DN, Wiestler OD, von Deimling A. Amplification of the cyclin-dependent kinase 4 (CDK4) gene is associated with high cdk4 protein levels in glioblastoma multiforme. Acta Neuropathol 1996;92:70–4.
51. Lo KC, Rossi MR, Burkhardt T, Pomeroy SL, Cowell JK. Overlay analysis of the oligonucleotide array gene expression profiles and copy number abnormalities as determined by array comparative genomic hybridization in medulloblastomas. Genes Chromosomes Cancer 2007;46:53–66.
52. Thompson MC, Fuller C, Hogg TL, et al. Genomics identifies medulloblastoma subgroups that are enriched for specific genetic alterations. J Clin Oncol 2006;24:1924–31.